Published in final edited form as:
Soft Matter. ; 19(30): 5692–5700. doi:10.1039/d3sm00673e.

Dynamic interfaces for contact-time control of colloidal interactions†

Yaxin Xu[a,*], **Kyu Hwan Choi**[a,*], **Sachit G Nagella**[a], **Sho C. Takatori**[a,‡]

[a]Department of Chemical Engineering, University of California, Santa Barbara, Santa Barbara, CA, USA.

Abstract

Understanding pairwise interactions between colloidal particles out of equilibrium has a profound impact on dynamical processes such as colloidal self assembly. However, traditional colloidal interactions are effectively quasi-static on colloidal timescales and cannot be modulated out of equilibrium. A mechanism to dynamically tune the interactions during colloidal contacts can provide new avenues for self assembly and material design. In this work, we develop a framework based on polymer-coated colloids and demonstrate that in-plane surface mobility and mechanical relaxation of polymers at colloidal contact interfaces enable an effective, dynamic interaction. Combining analytical theory, simulations, and optical tweezer experiments, we demonstrate precise control of dynamic pair interactions over a range of pico-Newton forces and seconds timescales. Our model helps further the general understanding of out-of-equilibrium colloidal assemblies while providing extensive design freedom via interface modulation and nonequilibrium processing.

1. Introduction

The material properties of colloidal suspensions depend on the multibody interactions between constituent particles.[1] These interactions may be programmed through functionalizing colloids with surface species such as DNA linkers[2–5] or polymer brushes[6,7] to guide or hinder colloidal aggregation. In modelling such systems, one typically assumes a separation of timescales between the rapid relaxation of surface species and the colloidal Brownian diffusion[8] to obtain an effective, ‘static’ pair potential, which solely depends on the instantaneous pair separation.[9,10] Although only exact at equilibrium, static potentials have been applied successfully to describe many colloidal suspensions out of equilibrium.

†Electronic Supplementary Information (ESI) available: See DOI: 10.1039/cXsm00000x/

‡Corresponding author: stakatori@ucsb.edu.
*Equal contribution

Author Contributions

Y.X., K.C., and S.C.T. conceived of the study, all authors designed research, Y.X. performed simulations and theoretical calculations, S.G.N. performed calculations of the fluid-mediated effects, K.C. performed experiments, S.C.T. supervised the study, and all authors wrote the paper.

Conflicts of interest

There are no conflicts of interest to declare.

In some cases, however, nonequilibrium processes such as hydrodynamic flows[11] or kinetic arrest[12] drive colloids together or apart faster than the surface species equilibration, resulting in a nontrivial interplay between the macroscopic process timescale and kinetics at the contact interface. For instance, the stiffening of particle-particle contacts in dense colloidal suspensions can lead to logarithmic growth in the elastic moduli over time, in the absence of microstructural changes.[13,14] Additionally, theoretical work has shown that suspensions of polymer-grafted particles can exhibit shear thickening through hydrodynamic interactions and contact relaxation.[15,16] Dynamical interactions are also biologically relevant; cell membranes are coated by receptors and biopolymers which spatially rearrange over cell-cell contact timescales of seconds to minutes to trigger T cell activation.[17,18] In these systems, a static potential is likely inadequate for predicting nonequilibrium pairwise interactions. By modulating the intrinsic timescales at colloidal contacts, we aim to engineer a dynamic pair potential for multiscale control of colloidal interactions out of equilibrium.

Consider the system in Fig 1: two colloids are coated by end-grafted polymers whose grafting sites are free to diffuse laterally along the surfaces. Colloids are brought to a small separation distance instantaneously and held fixed at those positions. Shortly after contact, colloids experience a strong steric repulsion due to polymer overlap between opposing surfaces. However, through grafting-site diffusion and chain relaxations at longer times, the polymers assume configurations that lower their overall energy, thereby reducing the effective repulsion experienced by the colloids. This contact-time dependent interaction relaxes over colloidal timescales and can affect overall suspension dynamics. Mechanistic understanding of these interactions has not been previously considered theoretically or experimentally.

In this work, we combine theory, simulations, and experiments to directly measure the force transmission between two colloidal particles coated by surface-mobile polymers as a function of their contact time. We find that the relaxation timescale of this dynamic interaction is modulated by nonequilibrium protocols such as colloid approach speed. Our mechanical understanding of dynamic pair interactions may help predict the out of equilibrium assembly of colloidal structures.

This paper is organised as follows. A brief overview of the theoretical model and simulations is presented in Section 2 and the experimental method is detailed in Section 3. In Section 4 we present results and analysis of contact-time dependent intercolloidal forces between two polymer-coated colloids as the system relaxes toward equilibrium and show how these interactions are precisely governed by nonequilibrium forcings. The paper closes with a discussion of these data in Section 5 as well as a simple demonstration of how surface modifications may be leveraged to engineer different types of dynamic interactions.

2 Theoretical Model

2.1 Smoluchowski Theory

For the system shown in Fig. 1, we now provide an overview of an analytical theory to capture relaxation dynamics of surface-bound, semi-rigid polymers. The probability density

$\rho(\mathbf{h}, t \mid H)$ of finding a monomer at position $\mathbf{h}$, given two colloids of size d_c at a separation H, satisfies the Smoluchowski equation:

$$\frac{\partial \rho}{\partial t} = -\nabla_h \cdot \mathbf{j} \tag{1}$$

where the flux contains thermal and interparticle contributions:

$$\mathbf{j} = -D_\rho \nabla_h \rho - D_\rho \rho \nabla_h V(\mathbf{h} \mid H)/k_B T\,. \tag{2}$$

Neglecting hydrodynamic interactions for now, D_ρ is simply the Stokes-Einstein-Sutherland (SES) diffusivity of the monomer. One may opt for a more sophisticated form of D_ρ for surface-mobile, end-grafted polymers, but we will use the SES diffusivity for simplicity. Assuming semidilute polymers, the interparticle potential $V = V_{\text{brush}} + V_{\text{HS}}$ is a sum of the entropic penalty of chain stretching and hard-core repulsion between monomers (see SI for functional forms). Normally, the translational motion of the colloids would also produce an advective particle flux contribution, $v\rho\mathbf{e}_x$, which scales with the approach velocity, v.[19–22] Because our model aims to capture the transient relaxation after colloidal motion has ceased ($v = 0$ for $t \geq 0$), we choose to set an initial, nonequilibrated concentration field to represent the state of monomers at $t = 0$ (see SI). Eq. 1 is numerically evaluated using the finite element software package FreeFEM++[23] for an arbitrarily-large 3-dimensional volume which includes both colloidal particles and the two polymer brush domains.

2.2 Brownian Dynamics Simulations

To validate our theoretical model, we also perform coarse-grained Brownian Dynamics (BD) simulations using HOOMD-Blue, a GPU-accelerated simulation package (Supp. Video 1–3).[24] All particles in the simulation follow the overdamped Langevin equation of motion:

$$\frac{\Delta \mathbf{x}_i}{\Delta t} = \left(\underbrace{\mathbf{F}_i^{\text{P}}}_{\text{interactions}} + \underbrace{\mathbf{F}_i^{\text{R}}}_{\text{Brownian}} \right) / \zeta \tag{3}$$

with contributions from interparticle interactions and thermal forces satisfying fluctuation dissipation theory. In Eq. 3, $\mathbf{x}_i$ is the position of particle i, and $\zeta = 3\pi\eta d_\rho$ is the drag coefficient. Polymers are modeled with identical properties using a Kremer-Grest bead-spring model with semi-flexibility,[25] where the grafting site is allowed to undergo diffusive translation along the surface (Fig. 1). To quantify the effective colloidal interaction mediated by brushes of mean height h_0, polymerization M and surface density n_ρ, we compute the force $\langle F(\mathbf{h}, t \mid H) \rangle$ exerted by polymers on the colloids along their line of centers, where $F = -n_\rho M \partial_H V$ and the brackets $\langle ... \rangle = \frac{1}{2}\int \rho ... d\mathbf{h}$. Polymer parameters and interactions with are chosen to match the experimental system (see SI).

3 Experimental Methods

In this section, we briefly summarize our experimental realization of surface-mobile polymer-coated colloidal particles and our interparticle force measurement technique.

All force measurements were conducted using the optical tweezer (OT) setup described in Fig. 2a.[26] Two polymer-grafted beads were held in two separate optical traps focused more than 40μm from the bottom cover slip. A supported lipid bilayer (SLB) containing dioleoyl-sn-glycero-3-phosphocholine (DOPC) was constructed on $d_c = 4\mu$m silica beads to enable mobility of surface species (Fig. 2b,d).[27] We chose filamentous actin (F-actin) as the grafted polymer for its ability to polymerize to large lengths[28] and well-known mechanical properties.[29,30] F-actin is known to polymerize to large length distributions,[28] and polymerization was quenched after reaching a length distribution of $2 - 20\mu$m by washing out unreacted materials. F-actin was end-grafted on the SLB by 6x-histidine tagged gelsolin to an anchoring lipid, 1,2-dioleoyl-sn-glycero-3-[(N-(5-amino-1- carboxypentyl)iminodiacetic acid)succinyl] (DGS-NTA(Ni)), which was doped in the bilayer over a range of 0 − 10% to vary F-actin surface density between $n_{\text{actin}} \approx 0 - 12,000/\mu\text{m}^2$ (Fig. 2c, Supp. Video 4, see SI for F-actin density characterization). The mean separation between grafting sites is 10 − 20nm, such that F-actin assumes a brush configuration. 1,2-dioleoyl-sn-glycero-3-phosphoethanolamine (DOPE) labeled with Atto-488 was added at 1% for fluorescence.

To characterize pair interactions out of equilibrium, a pair of colloids is placed in separate optical traps; one trap is stationary whereas the other trap translates at a fixed speed ($v = 0.5 - 10\mu\text{m}/s$) to bring the colloids from a large separation (35μm) to a closest distance of 400 − 500 nm before being fixed at this position for 20s (Fig. 2e, Supp. Video 5–6). We then measured the stationary colloid displacement about its trap center at every time step, dx, following $\langle F \rangle = F_{\text{trap}} = \kappa_t \cdot dx$, with a trap stiffness $\kappa_t = 0.5 - 0.7\text{pN}/\mu\text{m}$. During the approach step, we did not observe convection-induced accumulation of F-actin to the rear of the colloid (Supp. Video 6), indicating that hydrodynamic forces do not macroscopically perturb the polymer distribution.

4 Results

4.1 Brush-mediated interactions relax over timescale of colloidal contact

In Fig. 3a, we plot the force exerted between the colloids as a function of the inter-colloidal separation H for a family of contact times. The inset shows cross-sectional monomer density solutions to Eq. 1 - 2 for short and long contact times. At a given separation, we observe that the repulsive forces decay as a function of contact time. At small times, $t \ll d_c^2/D_\rho$, we observe a repulsive force that strengthens when brushes are fully overlapped, $(H - d_c) = h_0$, resulting from high osmotic pressure across the contact interface.[1] When the contact times exceed the diffusive timescale for the grafting site to explore the colloidal surface, $\tau_R \sim d_c^2/D_\rho$, polymers chains and their grafting sites have substantially depleted from the interfacial region, resulting in an order of magnitude decrease in force. Unlike static pair potentials, this dynamic interaction is unusual because the colloids' instantaneous separations do not fully capture their force and stress transmission. We also note that this dynamic interaction is governed by the intrinsic, diffusive timescales of the polymers and is distinct from externally-imposed, time-varying potentials.[31–33]

In the late stage, infinite time limit, taken to be $tD_p/d_c^2 = 20$, compressed polymers fully relax through diffusive redistribution of their grafting sites out of the contact interface and spatial reorganization of the polymer chain. In Fig. 3b, we plot the colloidal force as a function of contact time when colloids are in contact at the closest separation, $H = dc$. We show that the force decays exponentially towards the equilibrium value, suggesting a characteristic relaxation timescale associated with polymer reorganization over the colloidal surface. This relaxed force is weaker than static repulsion between polymer brushes whose grafting sites are not laterally mobile.[1,34–36] We find good agreement between theoretical predictions and our BD simulations despite the simplicity of our polymer model.

4.2 Surface-mobile F-actin mediates dynamic colloidal interactions

So far, we have demonstrated that a nonequilibrium interaction exists between colloids coated with surface-mobile polymer layers through a theoretical model and BD simulations. Next, we present the experimental realization of this system. In Fig. 4, we plot the interaction force against time for various approach velocities, where the translating trap stops motion at $t = 0$. We observed that the repulsive forces increase as the two colloids approach for times $t < 0$ due to F-actin interactions with the opposing colloidal surface, and is maximized at the closest separation, $\langle F(t = 0)\rangle = F_{\max}$. At the fastest approach velocity, $10\mu m/s$ (black curve), the repulsive force relaxes from $F_{\max}$ to the equilibrium force, F_{eq}, on an observable timescale, $\tau_R \approx 2.5$s, consistent with literature values for F-actin spatial reorganization over the colloidal size, $\tau_R \sim 4\mu m^2/D_a \approx 2.7$s, where $D_a = 1.5\mu m^2/s$ is F-actin diffusivity in solution.[37] We therefore rationalize that the in-plane fluidity of the membrane surface enables an exquisite control over the reorganization of F-actin at the contact interface and the force transmission between the colloids.

At slow approach velocities, 0.5μm/s, the repulsive force between the colloids immediately equilibrates — their interactions are quasi-static because the polymers have sufficient time to reorganize during every step of approach. This equilibrium force is related to a potential of mean force, $F_{0.5\mu m/s} = -\int \rho_{eq} \partial_H V d\mathbf{h}$ where $\rho_{eq} = e^{-V/k_B T}$ is the equilibrium monomer distribution, and is analogous to the infinite contact time limit of Fig. 3a where interfacial polymers have fully relaxed.

As a control, we show that the forces between SLB-coated colloids without F-actin remained approximately zero throughout, except for the small peak associated with a lubrication force at the largest velocity. The small negative $F_{eq} \approx 50$fN indicates a weak, van-der Waals-type attractions.

Figure 4 is an experimental realization of our simulations in Fig. 1 and 3, where two colloids placed quickly into contact experienced a repulsive force that decays with contact time. Using our membrane-coated colloids with different surface conditions, one can create a range of designer pair potentials with tunable contact-time interactions, as demonstrated theoretically in Fig. 3.

4.3 Nonequilibrium timescales compete with surface polymer relaxation

The contact-time dependent interactions in Fig. 3 and 4 arise from the nonequilibrium distributions of interfacial polymers. Therefore, any process that moves the colloids in and out of contact on a timescale that competes with polymer relaxation, such as hydrodynamic fluid flows and other non-conservative body forces, can induce a dynamic interaction. To understand the impact of these competing timescales, we systematically varied the approach velocities of the colloids leading to their closest separation.

In Fig. 5a, we measured the effective force as a function of approach velocity at a fixed colloidal separation ($H = 8\mu$m) for two actin surface densities, $12,000/\mu\text{m}^2$ and $3,000/\mu\text{m}^2$. We observe that the effective colloidal force increases for higher surface densities, consistent with our hypothesis that the polymer-mediated repulsion is induced by increased osmotic pressure (Fig. 3a, inset). Also, the forces generally increase for higher approach speeds, which we attribute to the degree of F-actin compression at the contact interface. During a "fast" approach ($v > 2\mu$m/s), F-actin of mean height $h_0 \sim 5\mu$m is compressed at a timescale $\tau_{\text{process}} \sim h_0/v = 2.5$s, which is comparable to the F-actin reorganization on the colloid surface. Thus, polymers compress without having sufficient time to explore favorable configurations. Higher approach speeds induce an increasingly dense layer of interfacial F-actin, generating stronger forces. This repulsion begins to plateau at the highest approach speed (10μm/s), possibly because polymers cannot infinitely accumulate. Note in Fig. 5a that the theoretical polymer configurations were generated for the initial approach (see SI for polymer initialization).

Our results confirm that faster approach processes drive polymers further away from their equilibrium distribution. Therefore, the approach timescale should not only influence the strength of polymer-mediated interactions but also control their relaxations toward equilibrium. In Fig. 5b, we plot the characteristic relaxation time τ_R of the effective force as a function of approach speed. In experiments, theory, and simulations, τ_R is taken to be the time for the instantaneous force to relax 90% toward the equilibrium value F_{eq} from the peak value, F_{max}. We observe that the relaxation time increases with faster approach speeds, suggesting that polymers equilibrate more slowly when strongly compressed.

Interestingly, the relaxation time is independent of the F-actin surface density (Fig. 5b). From our flux expression (Eq. 2), we conclude that it is the *gradients* in polymer concentration along the colloidal surfaces, $\nabla_{\mathbf{h}}\rho$, which drive relaxation towards equilibrium. This is reminiscent of Marangoni forces that drive surfactant molecules from high to low concentrations.[38] Such a trend supports our theoretical framework of modeling relaxation as a diffusion-mediated process, as opposed to other mechanisms that depend on polymer concentration.

4.4 Fluid-mediated effects on colloidal interactions

4.4.1 Lubrication approximation on bare particles—In Fig. 5, we have found that a free-draining model of the F-actin layer sufficiently captures the key physics behind our experimental trends. In general, however, fluid-mediated effects cannot be neglected. As a control, we now show that forces between SLB-coated colloids without F-actin scale linearly

with approach speed, which is consistent with low-Reynolds number hydrodynamics (Fig. 5a, Supp. Video 7).[39]

As shown in Fig. 2e, the moving bead is brought to the stationary particle at a fixed speed until they reach close contact. For bare, SLB-only colloids, the observed maximum in the force F_{max} primarily due to fluid-mediated hydrodynamic interactions. During the approach process, the translating colloid diverts fluid from the interfacial gap between it and stationary particle, generating viscous drag forces. When the interfacial gap thickness is much smaller than the particle radius, the pressure difference between the interface and the surrounding bulk medium increases significantly to expel fluid from the thin film. Reynolds considered the asymptotic limit of a sphere approaching a planar surface and determined that the hydrodynamic force scales sensitively with the aspect ratio between the gap size ε and the particle diameter d_c.[40] Equivalently, here we consider the two particles asymptotically approaching the symmetry plane between them, i.e. $\varepsilon \equiv (H - d_c)/d_c \ll 1$, such that, to leading order, the lubrication force due to the squeezing motion is given by $F^H \sim 3\pi\eta d_c v\varepsilon^{-1} + O(\ln(\varepsilon))$.[41]

In Fig. 6 we compare the measurements of F_{max} with the instantaneous velocities of the stationary bead v_1 along the direction of tweezer motion, computed from the displacement time-trajectories. The slope of the force-velocity data provides the hydrodynamic resistance. Upon closest approach ($H - d_c \approx 400$nm), the stationary particle moves away from the incoming bead due to the hydrodynamic force (see Supp. Video 7). When the moving particle stops translating, the stationary bead reverses its motion. This momentary configuration of the beads is convenient to analyze, as the moving particle is now held in place ($\mathbf{v_2} = \mathbf{0}$) while the stationary particle moves towards the laser focus at an instantaneous velocity $\mathbf{v_1}$. In general, there are additional resistances due to the coupling between the forces and rotations. For example, a torque-free particle can simply rotate in response to local shearing by the fluid flow, effectively reducing the translational resistance. However, in the thin-gap limit, the leading-order resistance due to the force-rotation coupling scales as $\ln(\varepsilon)$.[42] Therefore, we expect the force response on the stationary colloid to behave as

$$\mathbf{F}_1^{ext} \sim \zeta_c \varepsilon^{-1} \mathbf{v}_1 + O(\ln(\varepsilon)), \tag{4}$$

$\zeta_c = 3\pi\eta d_c$ is the colloidal drag coefficient. We calculated $\mathbf{F}_1^{ext} \approx 0.39\text{pN}/\mu\text{m/s}$ and find that experimentally, the bare particles is to within order of magnitude of the Reynolds prediction. The overestimation of the theoretical result may be attributed to neglecting the higher-order corrections to the hydrodynamic force between approaching spheres with and without rotations. By balancing the lubrication force with the optical tweezer force, we predict a short and constant relaxation time $\tau_{SLB} = 3\pi\eta d_c^2/(2\kappa_t(H - d_c)) \approx 1$s, in agreement with our experimental observations (Fig. 5b).

4.4.2 Effect of end-grafted F-actin on hydrodynamic resistance—

The addition of F-actin on the lipid bilayer surface increases the hydrodynamic resistance to solvent flow during bead approach (Fig. 6). We rationalize this enhancement in the observed resistance

by considering the increased viscous dissipation inside the polymer layer. Whereas the solvent flows unimpeded out of the interfacial volume for two bare beads, introducing the polymer layers sets up a locally porous medium that inhibits fluid flow. However, because increasing the surface density of F-actin corresponded to a larger interparticle separation at closest approach, the peak force measurements were not taken at small gap separations and straightforward application of lubrication theory will not demonstrate agreement with the experimental data. Should the gap separation be consistent with the compression of the end-grafted F-actin layers, we may refer to existing theories for a prediction of the hydrodynamic force.

Viscous flows through porous media are typically modeled using the Brinkman equation which accounts for the medium permeability by introducing a source term to the Stokes equations.[43] Fredrickson and Pincus applied a lubrication-type analysis of the Brinkman equation to determine the hydrodynamic force between two grafted polymer surfaces.[44] Modelling the local structure within the thin-gap as a semi-dilute polymer solution, they determined the permeability in terms of the equilibrium mean separation between chains and its dependence on gap separation (i.e., ε). While this hydrodynamic force scales as $F^{\mathrm{H}} \sim \varepsilon^{-\frac{1}{2}}$, a weaker dependence on the geometric aspect ratio than in the Reynolds result, the magnitude of the lubrication force is enhanced through incorporation of a polymer hydrodynamic screening length, ξ_{H}. This enhancement is consistent with the intuition that the polymer layer impedes fluid flow and is qualitatively observed through surface force measurements.[36,45] Such an analysis would be valid on the nonequilibrium process timescales which are slower than that of F-actin reorganization, so that the grafted layer behaves as a “static” mesh whose structure is unperturbed by fluid flow. Otherwise, one would have to self-consistently solve the Stokes equations with a model for the body force that couples to the polymer dynamics[46,47], which we will leave to future work.

5 Discussion

In this paper, we have demonstrated that functionalizing colloidal surfaces with laterally-mobile, end-grafted polymers generates a dynamic pair force which relaxes as a function of colloidal contact times. We observe that timescales of nonequilibrium processes driving colloids into contact non-trivially compete with the timescale of polymer brush reorganization away from the contact interface. Previous work has shown that F-actin in concentrated systems becomes rotationally immobile due to entanglement and hinderance by neighboring filaments.[48] At the surface concentrations probed in our study, the average distance between grafting sites is 10–20nm, versus the actin lengths of $O(\mu\mathrm{m})$). We do not expect surface-bound F-actin to pivot significantly about its anchoring point and relax through rotating away from the contact interface. We believe that slight deformations in the underlying lipid membrane by anchoring sites also cannot enable rotational mobility across the micrometer length scales of the contact interface.[49–51] Additional effects that can influence the net interaction include frictional forces between adsorbed polymer layers,[52–55] underlying lipid-membrane deformations due to anchoring proteins,[49–51] and fluid-mediated forces within polymer layers.[44,47,56] While a more accurate model that accounts for these interactions is left to future work, we have obtained proficient agreement between our

Smoluchowski theory with BD simulations and OT experiments. We believe our simple framework captures the essential nonequilibrium physics of polymer-mediated forces and relaxation at colloidal contacts.

We conclude this work by observing that surface chemistry and composition may be leveraged to engineer different types of contact-time dependent interactions. As a demonstration, we synthesize F-actin-coated colloids whose bilayers contain 1,2-dipalmitoyl-sn-glycero-3-phosphocholine (DPPC), which forms more rigid membranes compared to DOPC lipids.[57] Interestingly, the DPPC membrane organizes F-actin into rigid, protruding bundles with immobile and non-rotating grafting sites (Fig. 7a,b, Supp. Video 8). We surmise that micro-phase separation on the bead surface[58] induces gelsolin to form small patches, thereby organizing F-actin into bundles.

In Fig. 7c, we perform OT experiments to compare the effective colloidal force between DOPC and DPPC membrane conditions as a function of colloidal separation at a fixed approach speed (0.5μm/s). Unlike DOPC colloids, we observed sharp force increases and buckling when F-actin bundles on DPPC colloids begin to overlap, $H = 10\mu$m (Fig. 7c). Unlike the DOPC systems, the force profiles associated with F-actin on DPPC colloids do not demonstrate significant relaxation at velocities between $v = 0.5 - 10\mu\text{m}/s$. We hypothesize that the surface diffusion of F-actin on DPPC bilayers is significantly impeded by stiff bundle formation. Mechanistic understanding of the force transmission between bundle-forming F-actin layers is left for future work.

More generally, our conceptual framework of contact-time dependent interactions is applicable to systems beyond pair interactions of lipid-coated particles. For example, the interactions of a third colloid to a dimer would depend on surface rearrangement of mobile species. By extending to N-particle interactions, we can engineer the kinetics and morphology of multi-body assemblies. Our framework is also applicable to multi-component interfaces with adhesive linkers and repulsive brushes, analogous to ligand-receptor binding at crowded cell-cell junctions, and allows us to dynamic tune between repulsive and attractive interactions. More recently, explicit considerations of surface-mobile binding sites and their binding dynamics has been shown to influence colloidal self-assembly.[59,60] Understanding contact-time dependent pair interactions may assist the programmable design of higher-order structures in similar systems. The timescale competition between hydrodynamic shear and dynamic pair interactions may also impact particle suspension rheology.[61] Finally, our framework may help understand other complex dynamic interfaces such as surfactant-laden emulsions,[62,63] colloids coated by polymers with adsorption and desorption rates,[64,65] cell surfaces where proteins undergo lateral rearrangement upon cell-cell contact,[17] and uptake of macromolecules on membranes with characteristic wrapping times.[66]

Supplementary Material

Refer to Web version on PubMed Central for supplementary material.

Acknowledgements

We would like to thank Fyl Pincus, Eric Furst, Tim Lodge, Glenn Fredrickson, and Todd Squires for valuable discussions and feedback. This material is based upon work supported by the Air Force Office of Scientific Research under award number FA9550-21-1-0287. Y.X. acknowledges support from the Dow Discovery Fellowship at UC Santa Barbara. S.G.N. acknowledges support from the National Institutes of Health (1T32GM141846). S.C.T. is supported by the Packard Fellowship in Science and Engineering. Acknowledgment is made to the Donors of the American Chemical Society Petroleum Research Fund for partial support of this research. Use was made of computational facilities purchased with funds from the National Science Foundation (OAC-1925717) and administered by the Center for Scientific Computing (MR-SEC; NSF DMR 1720256) at UC Santa Barbara.

References

1. Russel WB, Saville DA and Schowalter WR, Colloidal Dispersions, Cambridge University Press, 1989.
2. Alivisatos AP, Johnsson KP, Peng X, Wilson TE, Loweth CJ, Bruchez MP and Schultz PG, Nature 1996 382:6592, 1996, 382, 609–611.
3. Santos PJ, Cheung TC and Macfarlane RJ, Nano Lett, 2019, 19, 5774–5780. [PubMed: 31348659]
4. Chen G, Gibson KJ, Liu D, Rees HC, Lee J-H, Xia W, Lin R, Xin HL, Gang O and Weizmann Y, Nature Materials, 2018.
5. Mirkin CA, Letsinger RL, Mucic RC and Storhoff JJ, Nature 1996 382:6592, 1996, 382, 607–609.
6. Biancaniello PL, Kim AJ and Crocker JC, Physical Review Letters, 2005, 058302.
7. Akcora P, Liu H, Kumar SK, Moll J, Li Y, Benicewicz BC, Schadler LS, Acehan D, Panagiotopoulos AZ, Pryamitsyn V, Ganesan V, Ilavsky J, Thiyagarajan P, Colby RH and Douglas JF, Nature Materials, 2009, 8, 354–359. [PubMed: 19305399]
8. Angioletti-Uberti S, Mognetti BM and Frenkel D, Physical Chemistry Chemical Physics, 2016, 18, 6373–6393. [PubMed: 26862595]
9. Loverso F, Egorov SA and Binder K, Macromolecules, 2012, 45, 8892–8902.
10. Egorov SA, Journal of Chemical Physics, 2008, 129, 64901.
11. Vermant J and Solomon MJ, Journal of Physics: Condensed Matter, 2005, 17, R187–R216.
12. Segrè P, Prasad V, Schofield A and Weitz D, Physical Review Letters, 2001, 86, 6042–6045. [PubMed: 11415424]
13. Bonacci F, Chateau X, Furst EM, Fusier J, Goyon J and Lemaître A, Nature Materials, 2020, 19, 775–780. [PubMed: 32123333]
14. Bonacci F, Chateau X, Furst EM, Goyon J and Lemaître A, Physical Review Letters, 2022, 128, 018003. [PubMed: 35061484]
15. Melrose JR and Ball RC, Journal of Rheology, 2004, 48, 937–960.
16. Melrose JR and Ball RC, Journal of Rheology, 2004, 48, 961–978.
17. Monks CRF, Freiberg BA, Kupfer H, Sciaky N and Kupfer A, Nature, 1998, 395, 82–86. [PubMed: 9738502]
18. Davis SJ and van der Merwe PA, Nature Immunology 2006 7:8, 2006, 7, 803–809.
19. Khair AS and Brady JF, Proceedings of the Royal Society A: Mathematical, Physical and Engineering Sciences, 2007, 463, 223–240.
20. Dzubiella J, Löwen H and Likos CN, Physical Review Letters, 2003, 91, 248301. [PubMed: 14683160]
21. Krüger M and Rauscher M, The Journal of Chemical Physics, 2007, 127, 034905. [PubMed: 17655461]
22. Dolata BE and Zia RN, Journal of Fluid Mechanics, 2018, 836, 694–739.
23. Hecht F, Journal of Numerical Mathematics, 2012, 20, 1–14.
24. Anderson JA, Glaser J and Glotzer SC, Computational Materials Science, 2020, 173, 109363.
25. Kremer K and Grest GS, The Journal of Chemical Physics, 1990, 92, 5057–5086.
26. Crocker JC, Matteo JA, Dinsmore AD and Yodh AG, Physical Review Letters, 1999, 82, 4352–4355.

27. Castellana ET and Cremer PS, Surface Science Reports, 2006, 61, 429–444. [PubMed: 32287559]
28. Sept D, Xu J, Pollard TD and McCammon JA, Biophysical journal, 1999, 77, 2911–2919. [PubMed: 10585915]
29. Claessens MM, Bathe M, Frey E and Bausch AR, Nature materials, 2006, 5, 748–753. [PubMed: 16921360]
30. Brangbour C, Du Roure O, Helfer E, Démoulin D, Mazurier A, Fermigier M, Carlier M-F, Bibette J and Baudry J, PLoS biology, 2011, 9, e1000613. [PubMed: 21541364]
31. Swan JW, Vasquez PA, Whitson PA, Fincke EM, Wakata K, Magnus SH, Winne FD, Barratt MR, Agui JH, Green RD, Hall NR, Bohman DY, Bunnell CT, Gast AP and Furst EM, Proceedings of the National Academy of Sciences, 2012, 109, 16023–16028.
32. Sherman ZM and Swan JW, ACS Nano, 2016, 10, 5260–5271. [PubMed: 27096705]
33. Tagliazucchi M and Szleifer I, Faraday Discussions, 2016, 186, 399–418. [PubMed: 26762675]
34. Dolan AK and Edwards SF, Proceedings of the Royal Society of London. A. Mathematical and Physical Sciences, 1974, 337, 509–516.
35. Milner ST, Science, 1991, 251, 905–914. [PubMed: 17847384]
36. Israelachvili JN, Intermolecular and surface forces, Academic press, 2011.
37. Janmey PA, Peetermans J, Zaner KS, Stossel TP and Tanaka T, Journal of Biological Chemistry, 1986, 261, 8357–8362. [PubMed: 3013849]
38. Leal LG, Advanced Transport Phenomena, Cambridge University Press, 2007.
39. Happel J and Brenner H, Low Reynolds number hydrodynamics: with special applications to particulate media, Springer Science & Business Media, 2012.
40. Reynolds O, Philosophical Transactions of the Royal Society of London, 1886, 177, 157–234.
41. Jeffrey DJ, Mathematika, 1982, 29, 58–66.
42. O'Neill ME and Stewartson K, Journal of Fluid Mechanics, 1967, 27, 705–724.
43. Brinkman HC, Flow, Turbulence and Combustion, 1949, 1, 23–34.
44. Fredrickson GH and Pincus P, Langmuir, 1991, 7, 786–795.
45. Klein J, Journal of the Chemical Society, Faraday Transactions 1: Physical Chemistry in Condensed Phases, 1983, 79, 99.
46. Doyle PS, Shaqfeh ES and Gast AP, Macromolecules, 1998, 31, 5474–5486.
47. Doyle PS, Shaqfeh ESG and Gast AP, Phys. Rev. Lett, 1997, 78, 1182–1185.
48. Sawyer WH, Woodhouse AG, Czarnecki JJ and Blatt E, Biochemistry, 1988, 27, 7733–7740. [PubMed: 3207704]
49. Brown MF, Biochemistry, 2012, 51, 9782–9795. [PubMed: 23163284]
50. Alas CD and Haselwandter CA, Physical Review E, 2023, 107, 024403. [PubMed: 36932542]
51. Rossy J, Ma Y and Gaus K, Current Opinion in Chemical Biology, 2014, 20, 54–59. [PubMed: 24815858]
52. Beltran-Villegas DJ, Edwards TD and Bevan MA, Langmuir, 2013, 29, 12337–12341. [PubMed: 24067114]
53. Swavola JC, Edwards TD and Bevan MA, Langmuir, 2015, 31, 9076–9085. [PubMed: 26223386]
54. Mari R, Seto R, Morris JF and Denn MM, Journal of Rheology, 2014, 58, 1693–1724.
55. Lin NYC, Guy BM, Hermes M, Ness C, Sun J, Poon WCK and Cohen I, Physical Review Letters, 2015, 115, 228304. [PubMed: 26650321]
56. Klein J, Kamiyama Y, Yoshizawa H, Israelachvili JN, Fredrickson GH, Pincus P and Fetters LJ, Macromolecules, 1993, 26, 5552–5560.
57. Rawicz W, Olbrich K, McIntosh T, Needham D and Evans E, Biophysical Journal, 2000, 79, 328–339. [PubMed: 10866959]
58. Chen D and Santore MM, Biochimica et Biophysica Acta (BBA)-Biomembranes, 2014, 1838, 2788–2797. [PubMed: 25064155]
59. McMullen A, Muñoz Basagoiti M, Zeravcic Z and Brujic J, Nature, 2022, 610, 502–506. [PubMed: 36171292]

60. Mitra G, Chang C, McMullen A, Puchall D, Brujic J and Hocky GM, Soft Matter, 2023, 19, 4223–4236. [PubMed: 37255223]
61. Wagner NJ and Russel WB, Physics of Fluids A: Fluid Dynamics, 1990, 2, 491–502.
62. Cristini V, Bławzdziewicz J and Loewenberg M, Journal of Fluid Mechanics, 1998, 366, 259–287.
63. Chesters AK and Bazhlekov IB, Journal of Colloid and Interface Science, 2000, 230, 229–243. [PubMed: 11017729]
64. Pincus P, Sandroff C and Witten T, Journal de Physique, 1984, 45, 725–729.
65. Pefferkorn E and Elaissari A, Journal of Colloid and Interface Science, 1990, 138, 187–194.
66. Nel AE, Mädler L, Velegol D, Xia T, Hoek EMV, Somasundaran P, Klaessig F, Castranova V and Thompson M, Nature Materials, 2009, 8, 543–557. [PubMed: 19525947]

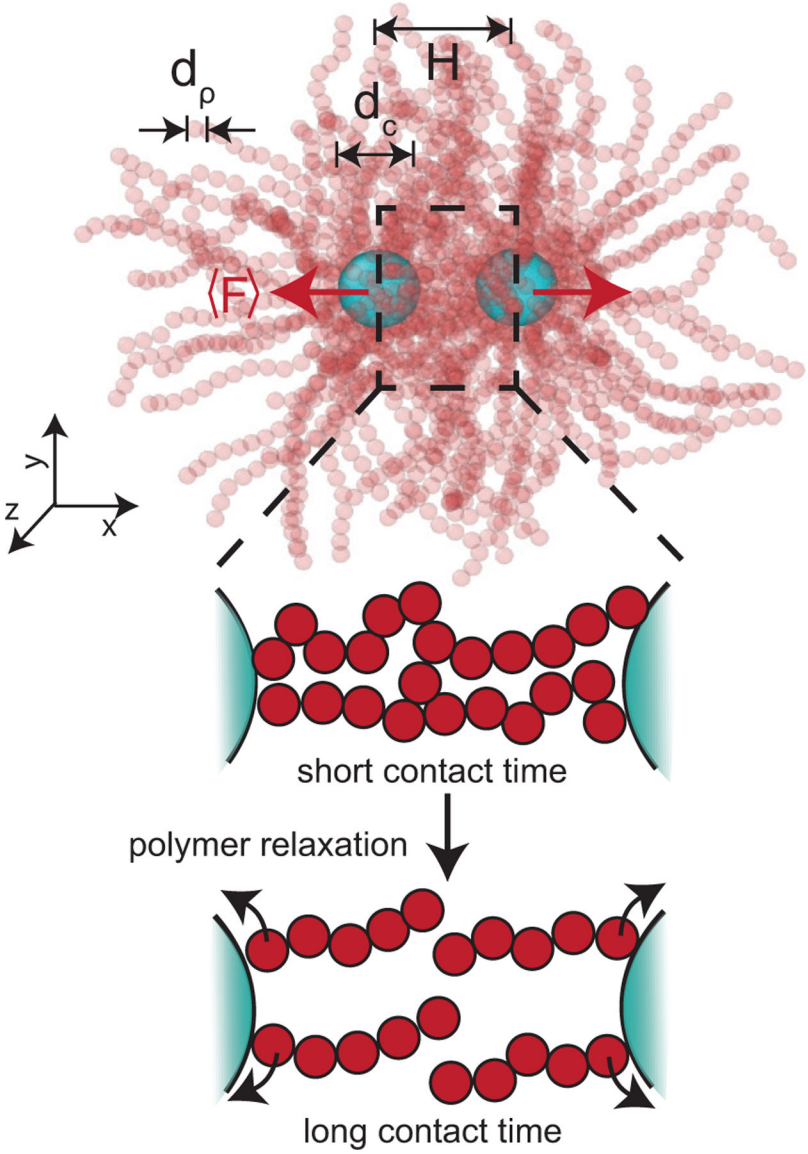

Fig. 1.

Brownian Dynamics (BD) snapshot of colloids coated with surface-mobile polymers. Two colloids (blue) with diameter d_c at separation H are coated by same-length, end-grafted polymers (red) with surface-mobile grafting sites, mean height h_0, bead diffusion coefficient D_ρ and bead diameter d_ρ. When the colloids are brought into a distance $H \ll 2h_0$ over a short timescale $\tau_{\text{process}} \ll d_c^2/D_\rho$, the polymers are forced into nonequilibrium configurations and generate a large effective force $\langle F \rangle$ between the colloids. As the polymers relax towards equilibrium, the effective interactions decay.

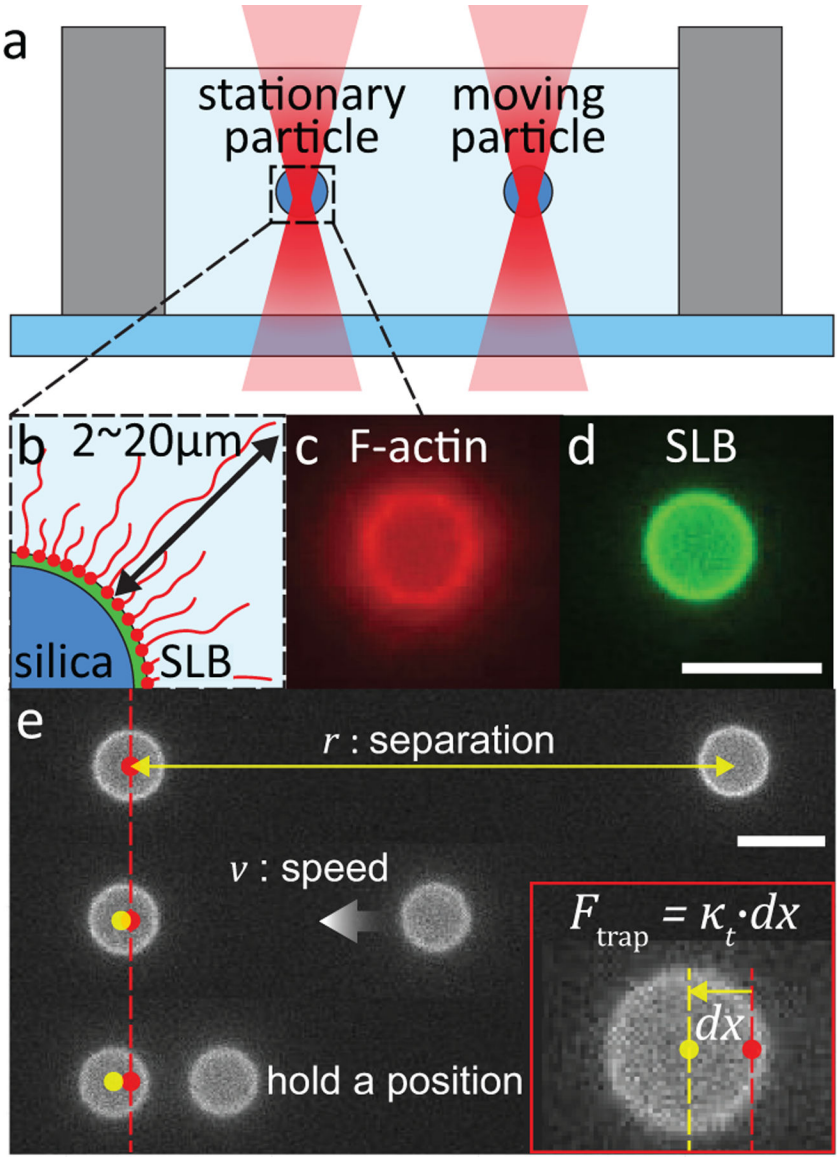

Fig. 2.

Experimental setup of a pair of Filamentous actin (F-actin) coated colloidal particles. (a) Schematic of optical laser tweezers and trapped particles in solution. (b) F-actin length ranges from 2μm to 20μm, with a mean $h_0 \approx 5\mu$m. (c,d) Fluorescence images of F-actin (red) bound to the lipid bilayer (green) containing polyhistidine tagged gelsolin and DGS-NTA(Ni). (e) Force measurement method. Inset shows the displacement from laser focus (red dot) to the mass center of the stationary colloid (yellow dot). All scale bars are 5μm.

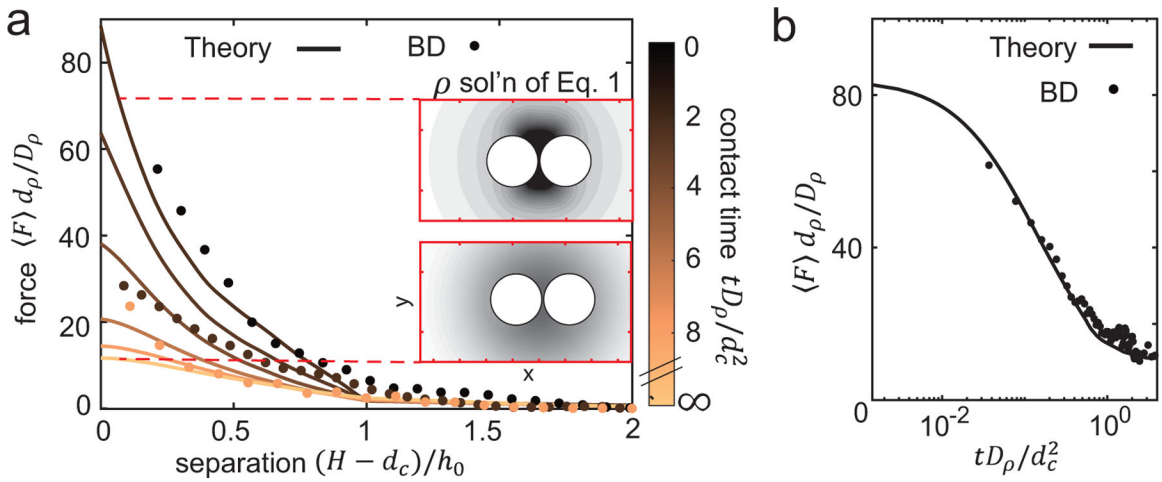

Fig. 3.

Effective repulsive forces between polymer-grafted colloids decay as a function of colloid-colloid contact time due to polymer relaxation at the contact interface. (a) Effective colloidal forces as a function of H for short (black) to long (yellow) contact times. Inset shows numerical solutions of Eq. 1–2 for polymer density ρ at short (top) and long (bottom) contact times, with the late stage, infinite time force measured at $tD_\rho/d_c^2 = 20$. Dark regions indicate higher polymer density. (b) Effective colloidal force as a function of contact time at colloidal contact, $H = d_c$. Solid lines are numerical solutions to Eq. 1–2, and markers are BD simulations.

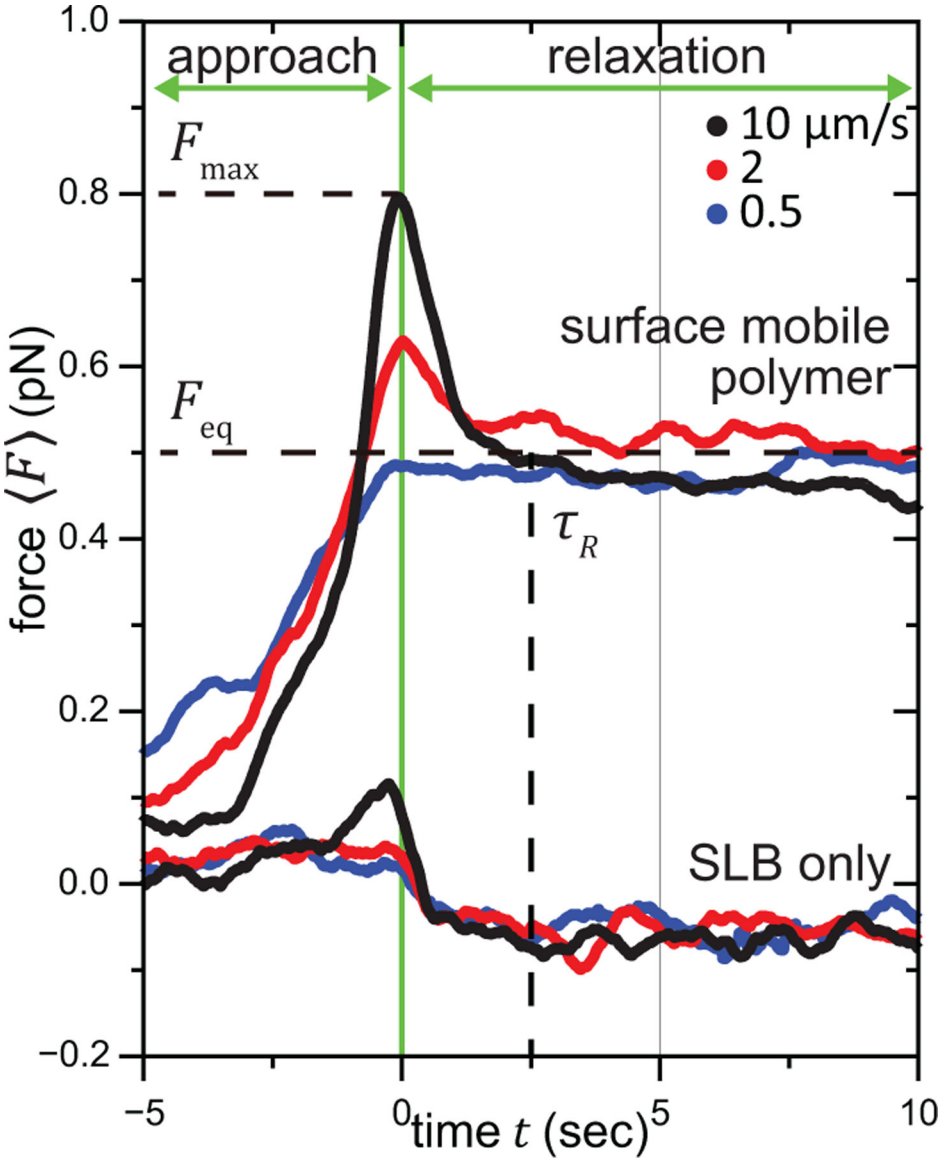

Fig. 4.

F-actin grafted on lipid bilayer-coated silica colloids generates contact-time dependent interactions between colloids. Plot shows force as a function of time on beads with F-actin surface density $n_{\text{actin}} \approx 12,000/\mu\text{m}^2$ and a separate measurement for bilayer-only control. Solid lines are time-average curves with approach speeds of $0.5\ \mu\text{m}/s$ (blue), $2\mu\text{m}/s$ (red), and $10\mu\text{m}/s$ (black), averaged over five colloidal pairs. Times $t < 0$ correspond to the approach step and $t \geq 0$ represent times when the colloids are at close contact (see SI Fig. 4).

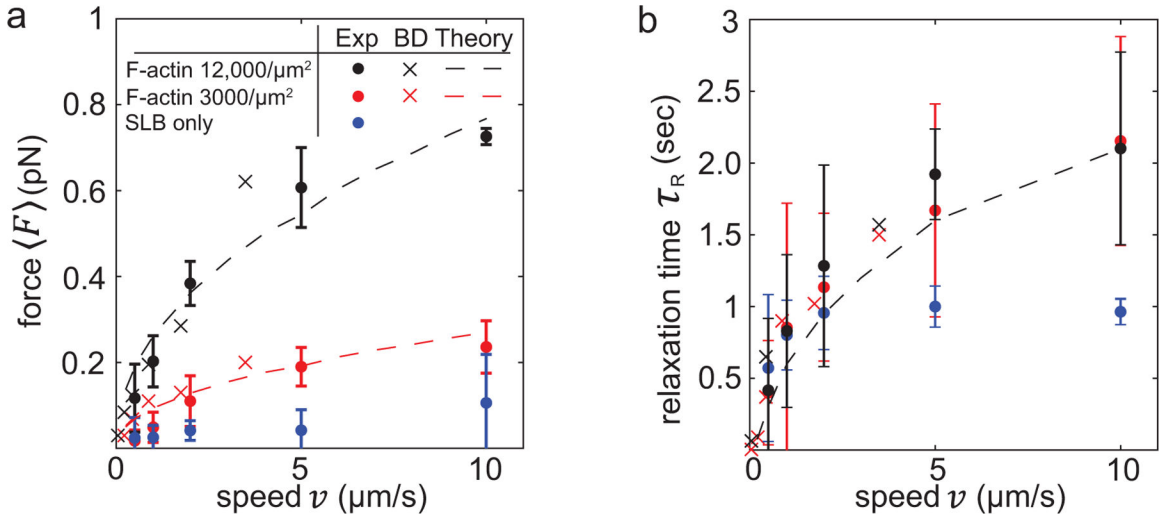

Fig. 5.

Nonequilibrium process timescale modulates strength and relaxation of dynamic colloidal interactions. (a) Effective colloidal force versus approach speed at a center-center separation of 8μm, for large actin density $\left(12,000/\mu\mathrm{m}^2\right)$ (black), moderate actin density $\left(3,000/\mu\mathrm{m}^2\right)$ (red), and SLB only (blue). (b) Relaxation time from peak force versus approach speed. Dashed curves are solutions to Eq. 1–2, filled circles are experiments, and crosses are BD simulations.

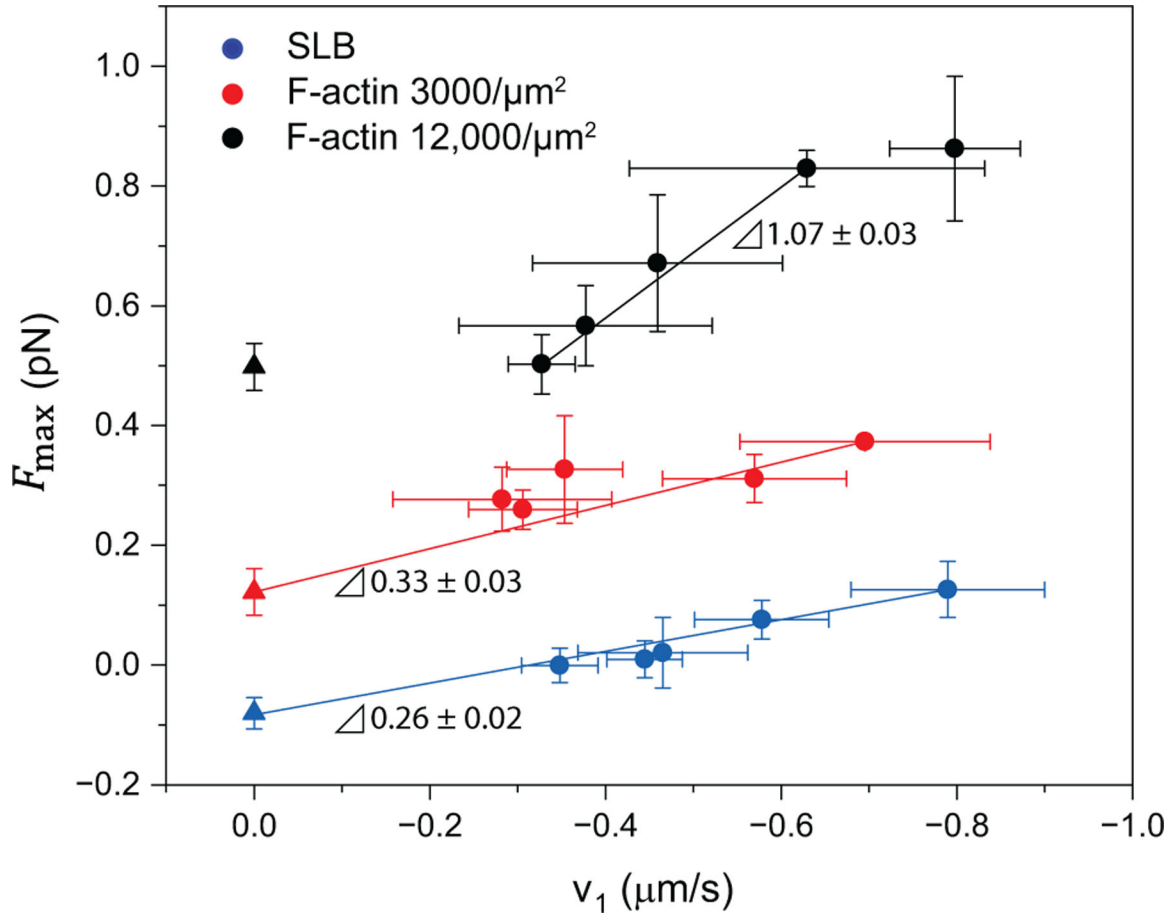

Fig. 6.

Maximum trapping forces on the stationary bead generally scale linearly with the instantaneous velocity v_1, upon closest approach with the moving particle. The instantaneous bead velocities v_1 were determined by time-differentiating the stationary bead displacements. Forces at $v_1 = 0$ are the equilibrium interactions between the particles, taken to be the "quasi-static" limit.

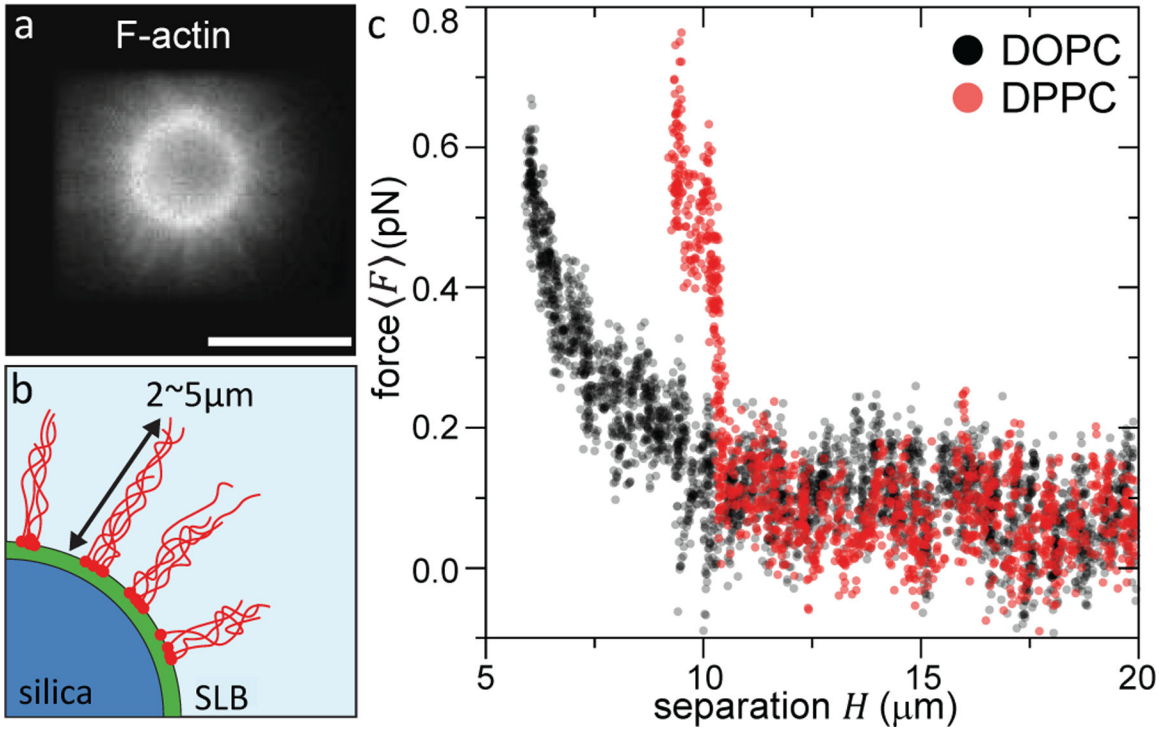

Fig. 7.

Less-mobile surface-grafted F-actin spontaneously organizes into rigid bundles, inducing steep and repulsive interactions which buckle when colloids are brought together. (a) Fluorescence image of end-grafted F-actin bundles coating the colloid whose SLB contains DPPC lipids and 10% DGS-NTA(Ni). All scale bars are 5μm. (b) Schematic of bundled F-actin with a mean bundle length 2μm, whose grafting sites are immobile, non-rotating, and phase-separated on the SLB surface. (c) Effective force changing in colloidal separation H when actin-coated colloids approach at 0.5μm/s. F-actin anchored to less-mobile DPPC SLB (red) mediates sharp force increases and buckling near $H = 10\mu$m, in contrast to monotonic repulsion when anchored to the more-mobile DOPC SLB (black).